




Metastatic prostate cancer-derived extracellular vesicles facilitate osteoclastogenesis by transferring the CDCP1 protein

Fumihiko Urabe^{1,2}  | Nobuyoshi Kosaka³ | Yusuke Yamamoto² | Kagenori Ito^{1,2} |
 Kurataka Otsuka^{2,3,4} | Carolina Soekmadji⁵  | Shin Egawa¹ | Takahiro Kimura¹ |
 Takahiro Ochiya³ 

¹Department of Urology, The Jikei University School of Medicine, Tokyo, Japan

²Laboratory of Integrative Oncology, National Cancer Center Research Institute, Tokyo, Japan

³Department of Molecular and Cellular Medicine, Institute of Medical Science, Tokyo Medical University, Tokyo, Japan

⁴R&D Division, Kewpie Corporation Sengawa Kewport, Tokyo, Japan

⁵School of Biomedical Sciences, Faculty of Medicine, University of Queensland, Brisbane, Australia

Correspondence

Takahiro Ochiya, Department of Molecular and Cellular Medicine, Institute of Medical Science, Tokyo, Japan.

Email: tochiya@tokyo-med.ac.jp

Present address

Nobuyoshi Kosaka, Pfizer Japan Inc, Tokyo, Japan.

Funding information

Japan Agency for Medical Research and Development, Grant/Award Number: JP21cm0106402; Japan Society for the Promotion of Science, Grant/Award Number: 21K16758; Japanese Urological Association, Grant/Award Number: Young Researcher Promotion Grant; Japanese Foundation for Prostate Research, Grant/Award Number: Researcher Promotion Grant; U.S. Department of Defense, Grant/Award Number: W81XWH-16-1-0736

Abstract

Bone metastases are still incurable and result in the development of clinical complications and decreased survival for prostate cancer patients. Recently, a number of studies have shown that extracellular vesicles (EVs) play important roles in tumour progression. Here, we show that EVs from metastatic prostate cancer cells promote osteoclast formation in the presence of receptor activator of NF- κ B ligand (RANKL). EV characterization followed by functional siRNA screening identified CUB-domain containing protein 1 (CDCP1), a transmembrane protein, as an inducer of osteoclastogenesis. Additionally, CDCP1 expression on plasma-derived EVs was upregulated in bone metastatic prostate cancer patients. Our findings elucidate the effect of EVs from metastatic prostate cancer cells on osteoclast formation, which is promoted by CDCP1 located on EVs. Furthermore, our data suggested that CDCP1 expression on EVs might be useful to detect bone metastasis of prostate cancer.

KEYWORDS

CDCP1, extracellular vesicles, osteoclast, prostate cancer

1 | INTRODUCTION

Prostate cancer (PCa) is the most frequently diagnosed male tumour and the second leading cause of cancer-related death in males in the United States (Siegel et al., 2021). PCa usually metastasizes to bone, and metastatic bone disease increases the risk of intractable bone pain, pathological skeletal fracture, and spinal-cord compression and decreases survival (Sturge et al., 2011). Therapeutic advances have been limited, and the most advanced stage of PCa remains incurable.

Bone is a dynamic organ that is constantly renewed by the balanced action of osteoblastic bone formation and osteoclastic bone resorption. This restructuring process called “bone remodelling” is important for the maintenance of bone mass and

This is an open access article under the terms of the [Creative Commons Attribution-NonCommercial-NoDerivs License](https://creativecommons.org/licenses/by-nc-nd/4.0/), which permits use and distribution in any medium, provided the original work is properly cited, the use is non-commercial and no modifications or adaptations are made.

© 2023 The Authors. *Journal of Extracellular Vesicles* published by Wiley Periodicals, LLC on behalf of the International Society for Extracellular Vesicles.

strength (Matsuo & Irie, 2008). However, once cancer cells metastasize to bone, the balance between osteoblasts and osteoclasts is disrupted. During bone metastatic progression, cancer cells stimulate osteoblasts to release receptor activator of NF- κ B ligand (RANKL). Osteoblast-derived RANKL binds to RANK, which is a receptor of RANKL expressed on osteoclast precursors. This heterotypic cell interaction induces the fusion of osteoclast precursors and the formation of mature multinucleated osteoclasts, resulting in enhanced bone resorption. Then, resorption of the bone matrix causes the release of growth factors such as insulin-like growth factor 1 (IGF-1) and transforming growth factor beta (TGF- β), leading to the progression of bone metastasis. This process is called the “vicious cycle” and has been widely accepted to establish osteolytic lesions to enhance bone metastatic progression (Guisse et al., 2006; Kingsley et al., 2007).

Despite emerging molecular discoveries, a more comprehensive understanding of bone metastasis is required to develop effective therapies. Indeed, denosumab, a fully human anti-RANKL monoclonal antibody, does not prolong survival in men with castration-resistant prostate cancer (CRPC) (Smith et al., 2012); therefore, an unknown molecular mechanism is likely involved in the progression of bone metastasis. Extracellular vesicles (EVs) are a heterogeneous family of vesicles that are generated from different subcellular compartments and released into extracellular space from almost all cell types. EVs function in intercellular communication by transferring intracellular contents, such as microRNA (miRNA), messenger RNA (mRNA), and proteins (Valadi et al., 2007). Previous reports have shown that EVs play important roles in tumour progression (Urabe et al., 2021). In this study, we found the effect of EVs isolated from metastatic PCa cells on mature osteoclast formation in the presence of RANKL and used functional siRNA screening to determine that CUB-domain containing protein 1 (CDCP1), which is a membrane protein located on EVs derived from PCa cells, promotes osteoclastogenesis. In addition, we found that high levels of CDCP1 were detected in plasma-derived EVs from PCa patients with bone metastasis.

2 | MATERIAL AND METHODS

2.1 | Cell line and cell culture

The human bone metastatic CRPC cell line PC-3 M-luc-C6 (PC3M) (Xenogen, Alameda, CA) and the immortalized normal human prostatic epithelial cell line PNT2 (DS Pharma Biomedical Co., Ltd., Osaka, Japan) were cultured in RPMI 1640 medium (Gibco, Waltham, MA) supplemented with 10% heat-inactivated fetal bovine serum (FBS) and antibiotic-antimycotic solution (Gibco) at 37°C. The murine monocytic cell line RAW264.7 was purchased from American Type Culture Collection. RAW264.7 cells were cultured in DMEM (Gibco) supplemented with 10% heat-inactivated FBS and antibiotic-antimycotic solution at 37°C. RAW264.7 cells were used at low passages (maximum +7 passages from purchase). Primary hematopoietic cells isolated from mouse bone marrow were cultured in α -MEM (Sigma Aldrich, St. Louis, MO) containing nucleosides, with the addition of 2 mM L-glutamine (Gibco), 10% heat-inactivated FBS, 100 U/mL penicillin, and 100 μ g/mL streptomycin (Gibco). For routine maintenance, each of the cell lines and the primary cells were grown as a monolayer at 37°C with 5% carbon dioxide and 95% relative humidity.

2.2 | Mouse study

The animal experiment in this study was performed in compliance with the guidelines of the Institute for Laboratory Animal Research, National Cancer Research Institute. Male BALB/c nude mice were purchased from Charles River Laboratories, Japan. Mice were maintained under sterile conditions in ventilated cages and racks with a 12 h light/12 h dark cycle. Male mice aged 5 weeks were used for intratibial tumour implantation. PC3M cells (1×10^5 cells/mouse) in 20 μ L of PBS were inoculated into the right tibia (20 μ L of PBS alone was inoculated into the left tibia). The mice were evaluated by *in vivo* imaging and microcomputed tomography (micro-CT) system R-mCT2 (Rigaku Co., Tokyo, Japan) 3 weeks after the injection.

2.3 | Preparation of conditioned medium and EVs

The cells were washed with phosphate-buffered saline (PBS), and the culture medium was replaced with Advanced RPMI 1640 medium (Gibco) for PC3M and PNT2 cells, containing an antibiotic-antimycotic mix and 2 mM L-glutamine. EVs from the conditioned medium were isolated by a differential ultracentrifugation protocol, as we previously reported (Yokoi et al., 2017). Briefly, the conditioned medium was centrifuged at $2000 \times g$ for 10 min to remove contaminating cells. The resulting supernatants were then transferred to fresh tubes and filtered through a 0.22 μ m filter (Millipore, Billerica, MA). The filtered conditioned medium was centrifuged for 70 min at $110,000 \times g$ using a SW41Ti rotor to pellet the enriched EVs (Beckman Coulter, Rea, CA). The pellets were washed with 11 mL of PBS and ultracentrifuged at $110,000 \times g$ for another 70 min using the SW41Ti rotor. The EV pellets were stored in a refrigerator at 4°C until use. The fraction containing the EVs was measured for its protein content using

the Quant-iT Protein Assay with the Qubit2.0 Fluorometer (Invitrogen, Carlsbad, CA) or Micro BCA protein assay kit (Thermo Scientific, MA, USA). The particle count and size distribution of EVs were determined using NanoSight system (NanoSight Ltd, Amesbury, UK). Samples diluted 100-fold with PBS were analysed using the NanoSight system LM10 with NTA2.3 Analytical software (NanoSight).

2.4 | Osteoclast differentiation

RAW264.7 cells were seeded in 48-well plates at a density of 1.0×10^4 cells per well with α -MEM containing 2 mM L-glutamine, 10% FBS, 100 U/mL penicillin and 100 μ g/mL streptomycin. After an initial attachment period of 12 h, the cells were cultured in the presence or absence of recombinant mouse RANKL (GST-RANKL, Oriental Yeast Co., Tokyo, Japan) at a concentration of 10 ng/mL alone or in combination with EVs for each period. Bone marrow cells were collected from the femurs and tibia of 6- to 10-week-old BALB/c nude mice (Charles River Laboratories Japan, Inc., Yokohama, Japan). The cells were centrifuged, and the harvested cells were cultured with α -MEM containing 2 mM L-glutamine, 10% FBS, and macrophage colony-stimulating factor (M-CSF, 10 ng/mL) for 16 h. Nonadherent mononuclear cells were collected, seeded on 150-mm culture dishes, and further incubated for 72 h with α -MEM containing 2 mM L-glutamine, 10% FBS, and M-CSF (50 ng/mL) to generate osteoclast precursor (OCP) cells. OCP cells were seeded into a 48-well plate (1.0×10^4 cells/well) and cultured in α -MEM culture medium in the presence or absence of RANKL (20 ng/mL) alone or in combination with EVs for 5 days with a change in culture medium every 2 days. On Day 6, the cells were stained with tartrate-resistant acid phosphatase (TRAP) using a TRAP Staining Kit (Cosmo Bio. Co., Ltd., Tokyo, Japan). TRAP-positive multinuclear cells containing three or more nuclei were counted as mature osteoclasts under a light microscope.

2.5 | Bone resorption assay

Bone resorption activities were determined by a bone resorption assay kit (Cosmo Bio. Co., Ltd.) based on the manufacturer's instructions. EV-induced bone resorption activity was evaluated by detecting the fluorescence intensity of conditioned medium at an excitation wavelength of 485 nm and an emission wavelength of 535 nm.

2.6 | Cell morphology analysis

For actin staining, osteoclast precursor cells were fixed with 4% paraformaldehyde for 10 min at room temperature. After washing with PBS, actin was stained with ActinGreen 488 Ready Probes Reagent (R37110, Molecular Probes). Then, after washing with PBS, the nuclei were stained with Hoechst 33342 (Dojindo, Kumamoto, Japan). The stained cells were washed in PBS for observation.

2.7 | siRNA transient transfection

A 2 mL PC3M cell suspension of 1.0×10^5 cells/well (in RPMI containing 10% FBS without antibiotics) was seeded into 6-well plates and incubated for 24 h. The transfection of 10 nM siRNA was accomplished using the DharmaFECT 1 transfection reagent (Thermo Fisher Scientific) according to the manufacturer's protocol. After 24 h, the medium was changed to Advanced RPMI 1640 medium containing an antibiotic-antimycotic mix and 2 mM L-glutamine. Forty-eight hours after the medium change, the conditioned medium was collected, and total RNA was extracted using the miRNeasy Mini Kit (Qiagen, Hilden, Germany) according to the manufacturer's instructions. The conditioned medium was purified for EV isolation by ultracentrifugation, and the total RNA was evaluated by qRT-PCR.

2.8 | Establishment of stable cell lines

A stable HEK293 cell line expressing CDCP1 was generated by selection with puromycin (2.5 μ g/mL). HEK cells at 90% confluency were transfected with the pCMV6-Myc-DDK-tagged ORF clone of human CDCP1 (Origene Technologies, Inc., Rockville, MD) and vector plasmid DNA in 24-well dishes using Lipofectamine 3000 reagent in accordance with the manufacturer's instructions (Invitrogen). Cells were replated in a 10-cm dish 24 h after transfection, followed by selection with 2 μ g/mL puromycin (Gibco) for 2 weeks.

2.9 | qRT-PCR

Total RNA (1.5 μ g) was isolated from the cell pellets using an RNeasy Mini Kit (Qiagen). RNA was converted to first-strand cDNA using the High-Capacity cDNA Reverse Transcription Kit (Applied Biosystems, Foster City, CA). Real-time PCR analyses were performed using StepOne Plus and TaqMan Universal PCR Master Mix (Thermo Fisher Scientific). mRNA expression was normalized to GAPDH expression. TaqMan probes for cathepsin K (CTSK) (Mm00484039_m1), dendritic cell-transmembrane protein (DC-STAMP) (Mm04209236_m1), TRAP (Mm00475698_m1) and GAPDH (Mm99999915_g1) were purchased from Applied Biosystems.

2.10 | Immunoblotting

Proteins were isolated from cells using M-PER (Thermo Scientific, MA, USA), separated in Mini-PROTEAN TGX Gel (5%–20%, Bio-Rad) and electrotransferred onto a PVDF membrane (Millipore). After blocking in Blocking One (Nacalai Tesque, Kyoto, Japan), the membranes were incubated for 1 h at room temperature with primary antibodies against the following antigens: CD9 (12A12, dilution 1:1000, COSMO BIO), CD63 (8A12, dilution 1:1000, COSMO BIO), CD81 (12C4, dilution 1:1000, COSMO BIO), nuclear factor of activated T-cells, cytoplasmic 1 (NFATc1) (#66963-1-Ig, 1:1000, Proteintech), RANKL (#ab9957, 1:1000), CDCP1 (#4115, 1:1000, Cell Signalling Technology), actin (C4, 1:5000, Millipore), and GAPDH (AB2302, 1:5000, Millipore). HRP (horseradish peroxidase)-linked secondary antibodies against mouse and rabbit immunoglobulin IgG (GE Healthcare) were used at a dilution of 1:5000. The membrane was then exposed to ImmunoStar LD (Wako, Osaka, Japan).

2.11 | RNA sequencing and analyses

The extracted total RNA was treated with RNase-free DNase I (Thermo Scientific, Waltham, MA), and the quality was tested using an Agilent 2100 Bioanalyzer (Agilent Technologies, USA). RNA sequencing (RNA-seq) libraries were prepared with the Illumina TruSeq Stranded mRNA protocol and sequenced on a HiSeq 2500 machine as paired-end, 100 base pair (bp) reads. Raw RNA-seq data were subjected to FastQC quality control. The sequencing data were analysed by using the software package Hisat2 and aligned to the reference genome human GRCh38. Expression quantified by normalization of the number of reads was defined as FPKM by Partek Genomic Suite version 6. The GEO accession number of our RNA-seq is GSE199912.

2.12 | PKH67-labeled EV transfer

Purified EVs derived from PC3M and PNT2 cells were labelled with the PKH67 Green Fluorescent Labelling Kit (Sigma–Aldrich). EVs were incubated with 2 μ M PKH67 for 5 min, washed four times through a 100-kDa filter (Microcon YM-100, Millipore) to remove excess dye, and incubated with RAW264.7 cells in the presence of RANKL (10 ng/mL) at 37°C.

2.13 | Proteome analysis of EVs

Protein solution samples were reduced and alkylated as previously described (Peng et al., 2011). Proteins were diluted 3-fold with 50 mM ammonium bicarbonate, pH 8.5, and digested with trypsin at an enzyme-to-substrate ratio of 1:50 (wt/wt, modified sequencing grade, Promega, Madison, Wisconsin, United States) for 16 h at 30°C. LC–MS/MS analyses were performed by nano LC (UltiMate 3000) (Dionex, Sunnyvale, CA, USA) coupled with a Q Exactive Plus Orbitrap mass spectrometer (Thermo Scientific, Waltham, MA, USA). Mass spectrometric analysis was performed according to a method described previously (Yamanaka et al., 2007). The database search was performed with MASCOT Deamon (Matrix Science, London, UK). The generated pkl files were submitted to NCBIInr (20130316). The search parameters were as follows: fixed modifications, carbamidomethyl; variable modifications, oxidation (M); missed cleavages, up to 1; monoisotopic peptide tolerance, 1.0 Da; and MS/MS tolerance, 0.5 Da. To eliminate the very-low-scoring random peptide matches automatically, the ion score cutoff was set to 30. The output data were analysed using Scaffold software version 4.8.4 (Proteome Software Inc., Portland, OR, USA).

2.14 | Electron microscopy

EVs purified from PC3M and PNT2 cells were observed using phase contrast electron microscopy, as described in our previous report (Kosaka et al., 2013). For immunoelectron microscopy, EVs were allowed to adsorb on nickel grids at room temperature.

Thereafter, the grids were incubated with primary antibody (anti-CDCP1, DY2666, R&D Systems, Inc.) in 1% BA-PBS for 2 h at room temperature, and the grids were washed with 1% BSA-PBS. The grids were subsequently incubated with secondary antibody conjugated to 10-nm gold particles (goat anti-mouse IgG polyclonal antibody, British BioCell International) for anti-CDCP1 antibody detection for 90 min at room temperature. After being washed with PBS, the grids were placed in 2% glutaraldehyde in PBS. Subsequently, the grids were stained with 2% phosphor tungstic acid solution (pH 7.0) for 15 s. The grids were observed by a transmission electron microscope (JEM-1400Plus; JEOL) at an acceleration voltage of 80 kV.

2.15 | Patient plasma samples

The collection and usage of human plasma from prostate cancer patients at The Jikei University School of Medicine were approved by the Institutional Review Board (No. 29–271(8887)). Plasma was aliquoted and stored at -80°C until use, and freeze–thawing was avoided thereafter. Informed consent was obtained from all patients. For immunoblotting, plasma samples were centrifuged at $10,000 \times g$ for 10 min at 4°C to remove cells and debris. To prepare EVs, the supernatant was ultracentrifuged at $210,000 \times g$ using a TLS-55 rotor for 35 min at 4°C (Beckman Coulter, Rea, CA). The pellets were washed with 2 mL PBS by ultracentrifugation at $210,000 \times g$ using a TLS-55 rotor for 35 min at 4°C . The EV pellets were stored in a refrigerator at 4°C until use.

2.16 | Statistical analysis

The data presented in the bar graphs are the mean \pm s.d. of at least three independent experiments. Student's *t*-test or an unpaired *t* test was used for comparison of two datasets. Analysis of variance (ANOVA) was used for multiple comparisons, followed by Dunnett's test or Bonferroni correction. The statistical software used was Prism version 7 (GraphPad Software, San Diego, CA). $p < 0.05$ was considered to be statistically significant. For analysis of LC–MS/MS data, Fisher's exact test was performed ($p < 0.003$).

3 | RESULTS

3.1 | Prostate cancer-derived EVs promote osteoclastogenesis

First, the human bone metastatic CRPC cell line PC3M, which can grow in bones and elicit an osteolytic reaction, was implanted via an intratibial injection to confirm the bone phenotype. Three weeks later, three-dimensional bone imaging was performed using micro-CT, and an osteolytic bone lesion was detected in the *in vivo* imaging system (IVIS)-positive area (Figure 1a). This osteolytic phenotype prompted us to focus on the relationship between cancer cells and osteoclasts. Previous studies have shown that several soluble factors in conditioned medium can induce osteoclastogenesis (Yuen et al., 2010). Therefore, we hypothesized that EVs derived from PCa also promote osteoclastogenesis. To observe the role of PC3M-derived EVs in osteoclastogenesis, the murine monocytic cell line RAW264.7, which has the potential to differentiate into osteoclast-like cells, was cultured with PC3M-derived EVs. As shown in Figure 1b, mature, three or more multinucleated, osteoclast formation was observed 96 h after the addition of RANKL. On the contrary, TRAP-positive cells containing a single nucleus were observed after the addition of PC3M-derived EVs only. As the mature osteoclasts are defined as TRAP positive multinucleated cells, these cells were not counted (Figure 1b). Indeed, TRAP positive multinucleated cells were not observed 168 h after the addition of PC3M-derived EVs only (Figure 1c). Then, to evaluate osteoclast differentiation and maturation, we classified TRAP-positive cells into three groups by the number of nuclei, and the number of TRAP-positive cells was compared in each group from 24 h to 168 h (Figure 1c). Although PC3M-derived EVs alone did not promote the formation of mature osteoclasts, PC3M-derived EVs in combination with RANKL significantly promoted the formation of mature osteoclasts compared with RANKL only (Figure 1b, c). Furthermore, several recent articles reported that filopodia in osteoclast precursors play important roles not only in cell migration but also in the perfusion selectivity of two osteoclast precursor cells (Irie et al., 2017; Song et al., 2014). RAW264.7 cells that were cocultured with PC3M-derived EVs in combination with RANKL formed numerous protruding long filopodia compared to those treated with RANKL alone (Figure 1a). Indeed, the osteoclast precursors, which have five or more filopodia, significantly increased after 72 h when osteoclast precursors were cocultured with PC3M-derived EVs in combination with RANKL (Figure 1b). During differentiation, more cell-to-cell contact via filopodia was observed with the treatments (Figure 1c). As osteoclasts matured, fewer filopodia were observed in osteoclasts at 120 h (Figure 1b). In addition, to investigate bone resorption activity, we performed a bone resorption assay by measuring chondroitin sulphate secreted due to osteoclast bone resorption. Bone resorption activities, as indicated by fluorescence intensity, were significantly enhanced in RAW264.7 cells that were cocultured with RANKL and PC3M-derived EVs compared to those cultured with RANKL only (Figure 1d).

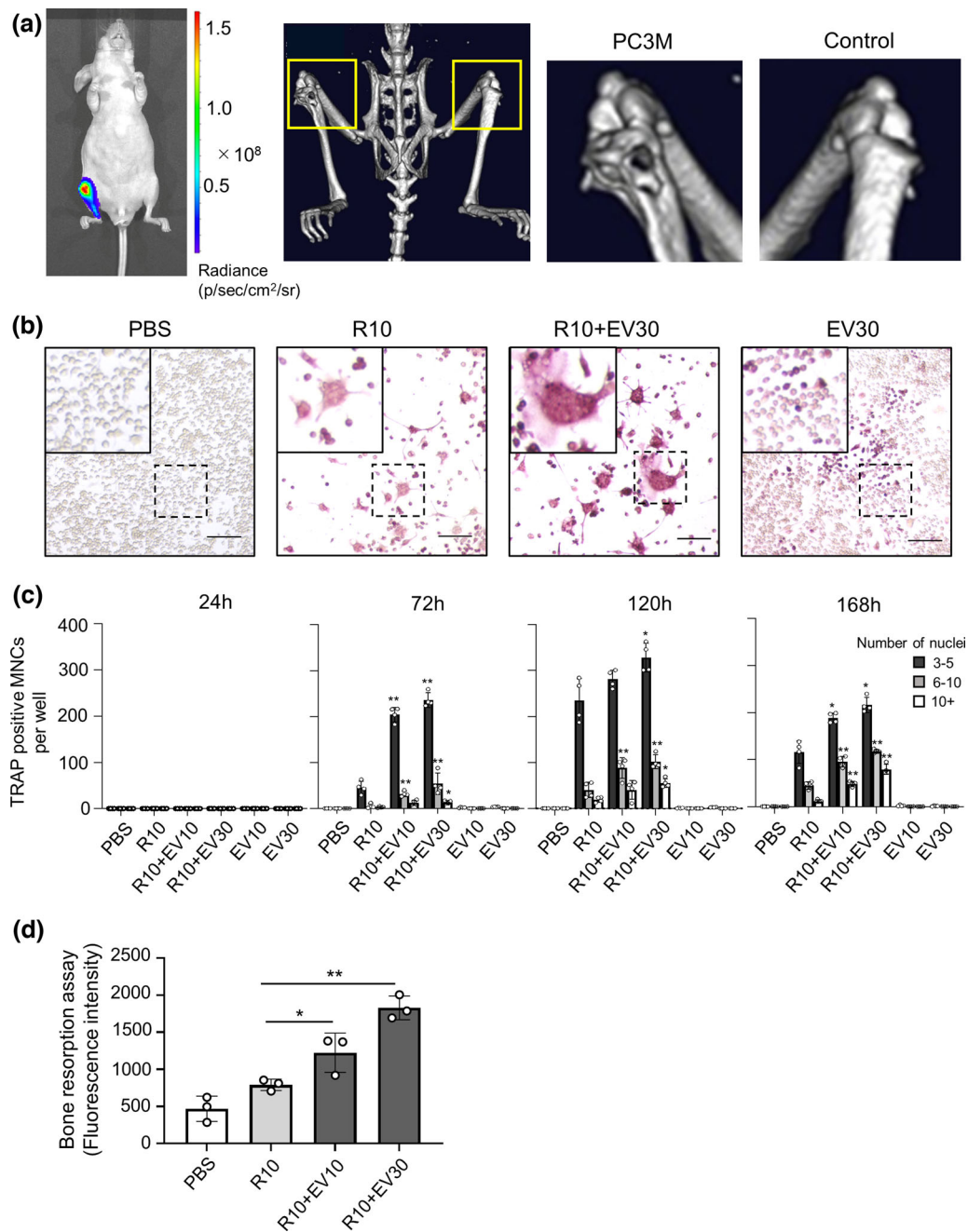


FIGURE 1 Prostate cancer-derived EVs promote osteoclastogenesis. (a) Intratibial tumours were evaluated by the photon radiance of the cancer cell bioluminescence (left panel). Microcomputed tomography (μ CT) revealed the same area as the osteolytic tumour site (yellow arrow in right panel). (b) Osteoclast precursor (RAW264.7) cells were cultured with EVs derived from PC3M cells with or without RANKL. At the end of Day 4, osteoclast precursor-induced cells were fixed, stained for TRAP, and observed under a light microscope. Scale bar, 100 μ m. The enlarged images are shown at the upper left of each image. (c) Osteoclast precursor cells were cultured with EVs derived from PC3M cells with or without RANKL. At different time points, osteoclast precursor-induced cells were fixed and stained for TRAP, and the number of TRAP-positive multinucleated cells containing more than 3 nuclei (MNCs) was counted. (d) The effect of PC3M-derived EVs on bone resorption activity of osteoclasts was evaluated by fluorescence intensity. Error bars represent s.d. of triplicate experiments. * and ** indicate significant differences from the RANKL-stimulated group (R10) as determined by Dunnett's test (* $p < 0.05$, ** $p < 0.01$). R10 represents 10 ng/mL RANKL, EV10 represents 10 μ g/mL PC3M-derived EVs, and EV30 represents 30 μ g/mL PC3M-derived EVs.

We next examined the effects of PC3M-derived EVs on osteoclast formation using primary osteoclast precursor cells. Bone marrow monocytes (BMMs) from BALB/c mice treated with 30 ng/mL M-CSF for 3 days were cocultured with 10 ng/mL RANKL, 50 μ g/mL M-CSF and PC3M-derived EVs for an additional 5 days (Figure S2a). TRAP staining was performed, and the number of mature osteoclasts was counted (Figure S2b). The results suggested that EVs from metastatic PCa cells facilitate osteoclastogenesis in the presence of RANKL.

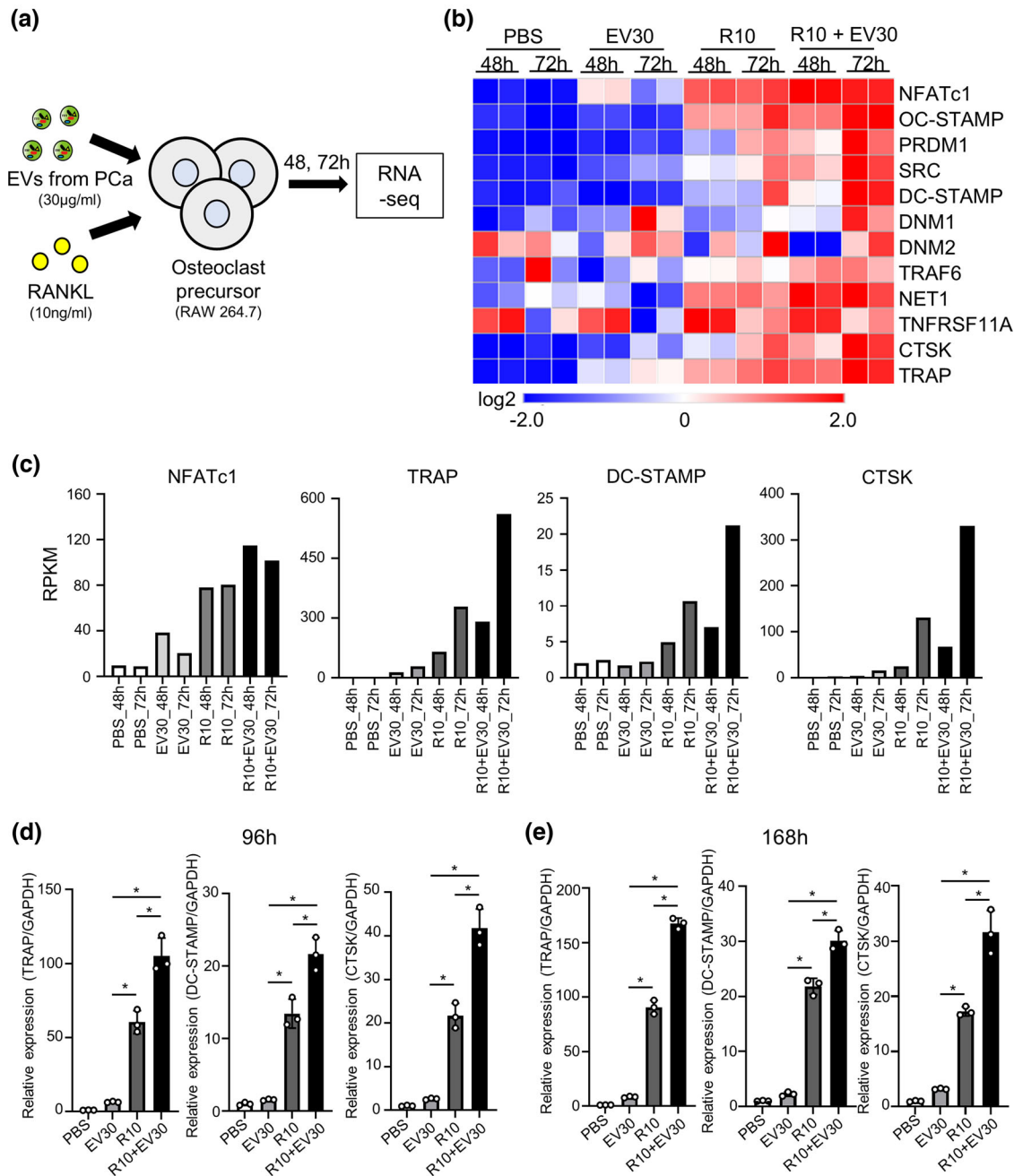


FIGURE 2 RNA-seq confirmed osteoclastogenesis induced by prostate cancer-derived EVs. (a) Schematic protocol for the gene expression analysis in osteoclast precursor cells (RAW264.7 cells) that were treated with EVs derived from PC3M cells (30 $\mu\text{g}/\text{mL}$) and RANKL (10 ng/mL). (b) Heatmap showing the difference in the expression level of mRNA that was previously reported to be related to osteoclastogenesis between osteoclast precursor cells treated with EVs derived from PC3M cells and RANKL. (c) The difference in NFATc1, TRAP, DC-STAMP and CTSK expression between the samples. The y-axis represents the expression level of the transcript quantified as reads per kilobase of the transcript per million mapped reads to the transcriptome (RPKM). (d) Osteoclast precursor cells were cultured with EVs derived from PC3M cells (30 $\mu\text{g}/\text{mL}$) with or without RANKL (10 ng/mL). After 96 h incubation, quantitative PCR analysis was performed for markers of osteoclast differentiation, including TRAP, DC-STAMP and CTSK. (e) Quantitative PCR analysis was performed for markers of osteoclast differentiation, including TRAP, DC-STAMP and CTSK after 168 h incubation. Error bars represent s.d. of triplicate experiments. Corrections passed the Bonferroni threshold ($p < 0.05/3 = 0.0167$) are marked with asterisk (*). R10 represents 10 ng/mL RANKL, EV10 represents 10 $\mu\text{g}/\text{mL}$ PC3M-derived EVs and EV30 represents 30 $\mu\text{g}/\text{mL}$ EVs.

3.2 | Whole transcriptome analysis reveals EV-regulated osteoclastogenesis

We found that EVs from metastatic PCa cells promote mature osteoclast formation in the presence of RANKL. Next, to examine the changes in gene expression in osteoclast precursors after the addition of PC3M-derived EVs, we performed RNA-seq (Figure 2a). As shown in the heatmap, the influence of RANKL in osteoclast differentiation was robust (Figure S3a). However,

RNA-seq revealed that PC3M-derived EVs additively upregulated the expression of genes associated with osteoclast differentiation in the presence of RANKL, although PC3M-derived EVs alone did not (Figure 2b). In particular, NFATc1, which is a master transcription factor in osteoclastogenesis, regulates the expression level of various factors affecting osteoclast formation, such as DC-STAMP, TRAP, and CTSK (Matsumoto et al., 2004; Teitelbaum & Ross, 2003; Yagi et al., 2006). These genes were upregulated in RAW264.7 cells after 48 or 72 h of coculture with PCa-derived EVs in the presence of RANKL (Figure 2c). Additionally, when RAW264.7 cells were incubated with the combination of RANKL and PC3M-derived EVs for 96 and 168 h, increased mRNA levels of the genes were confirmed by qRT-PCR (Figure 2d, e). In primary osteoclast precursors, the expression levels of TRAP and CTSK were still upregulated after 5 days of coculture with PC3M-derived EVs in the presence of RANKL (Figure S2c).

In addition, osteoclast precursor cell migration is a prerequisite for cell–cell contact and fusion prior to the formation of multinuclear osteoclasts (Irie et al., 2017). Prior to cell–cell fusion, osteoclast precursors protrude “neurite-like” filopodia and contact their neighbouring precursor cells (Figure S1a); Rho GTPases are important players in controlling this differentiation process (Song et al., 2014). RhoU, RhoF and Rac2 have been reported to regulate the formation and action of filopodia (Song et al., 2014), and the expression levels of these genes were greater after the addition of EVs in the presence of RANKL compared to expression after the addition of RANKL only (Figure S3b, c). From the point of whole transcriptome analysis, these results confirmed the occurrence of osteoclast differentiation and that the formation of filopodia was promoted by the addition of PC3M-derived EVs in the presence of RANKL.

3.3 | Normal prostate epithelial cell-derived EVs did not promote osteoclastogenesis

To further elucidate the effects of PC3M-derived EVs on mature osteoclast formation, EVs from the metastatic PCa cell line PC3M or from the normal prostatic epithelial cell line PNT2 were added to RAW264.7 cells. The vesicular structures of the EVs isolated from PC3M and PNT2 cells were observed by electron microscopy (Figure 3a). NTA analysis was performed to determine the size distribution of the EVs, which was approximately 30–250 nm, with a peak at approximately 70 nm (Figure 3b). In addition, we confirmed the enrichment of the known EV markers CD9, CD63 and CD81 by immunoblotting (Figure 3c). Although the abundance of CD63 was low in PNT2 cell-derived EVs, high levels of the other markers were detected in both EVs. These results are consistent with our previous report (Yoshioka et al., 2013). Furthermore, we observed the uptake of EVs derived from PC3M and PNT2 cells into RAW264.7 cells using PKH67-labeled EVs, and fluorescence was observed by confocal microscopy (Figure 3d). We next studied the effects of PC3M and PNT2 cell-derived EVs on mature osteoclast formation. RAW264.7 cells were cocultured with PC3M-derived EVs or PNT2-derived EVs in the presence of RANKL for 4 days. EVs derived from PC3M cells significantly promoted mature osteoclast formation, while PNT2-derived EVs did not induce osteoclastogenesis (Figure 3e). The interaction of RANKL with RANK on the osteoclast precursor cell membrane induces the initial expression of the master regulator of osteoclastogenesis, NFATc1 (Boyle et al., 2003). Therefore, we performed immunoblotting to determine whether PC3M-derived EVs contained RANKL or NFATc1, and we found that these proteins were not found in PC3M-derived EVs (Figure 3f). Collectively, these results suggested that the molecules contained in or on PC3M-derived EVs specifically promoted mature osteoclast formation in the presence of RANKL.

3.4 | EV characterization and functional siRNA screening to identify CDCPI

The cargo of EVs, which includes multiple biological components, is transferred from donor to recipient cells and influences the cellular phenotypes. Our data strongly demonstrated that EVs play an important role in bone resorption via RANKL-driven osteoclast differentiation, in which the presence of EVs induces bone resorption (Figure 1d). Next, we investigated which cargo of EVs is critical in promoting mature osteoclast formation.

In this study, to reveal the proteins in or on EVs that promote osteoclastogenesis, we performed proteome analysis. Isolated PC3M- and PNT2-derived EVs were subjected to LC–MS/MS analysis (Figure 4a). A total of 822 proteins were identified from these EVs, of which 119 and 56 proteins were specifically identified in PC3M- and PNT2-derived EVs, respectively (Figure 4b). To elucidate the biological functions of PC3M-derived EVs, proteins significantly expressed in PC3M-derived EVs were obtained from the 822 proteins and analysed by Fisher’s exact test (Figure 4c). As a result, 21 proteins were found to be significantly more prevalent in PC3M-derived EVs than in PNT2-derived EVs, and these proteins were thought to be candidate proteins that promote mature osteoclast formation (Figure 4c).

To determine which of these proteins is essential to mediate osteoclastogenesis in the presence of RANKL, we conducted small-scale screenings using an siRNA SMART pool in PC3M cells for the candidate proteins to promote osteoclast formation (Figure 4d). All Stars Negative Control siRNA (Qiagen) was transfected into PC3M cells, which were used as a positive control. We planned to perform three screenings to narrow down the reliable molecules. After excluding the proteins with concentrations in the EVs lower than 10 µg/mL, we performed screenings as shown in Figures 4e and S4a. Through this process, we found that EVs derived from CDCPI-downregulated PC3M cells did not promote mature osteoclast formation even in the presence of

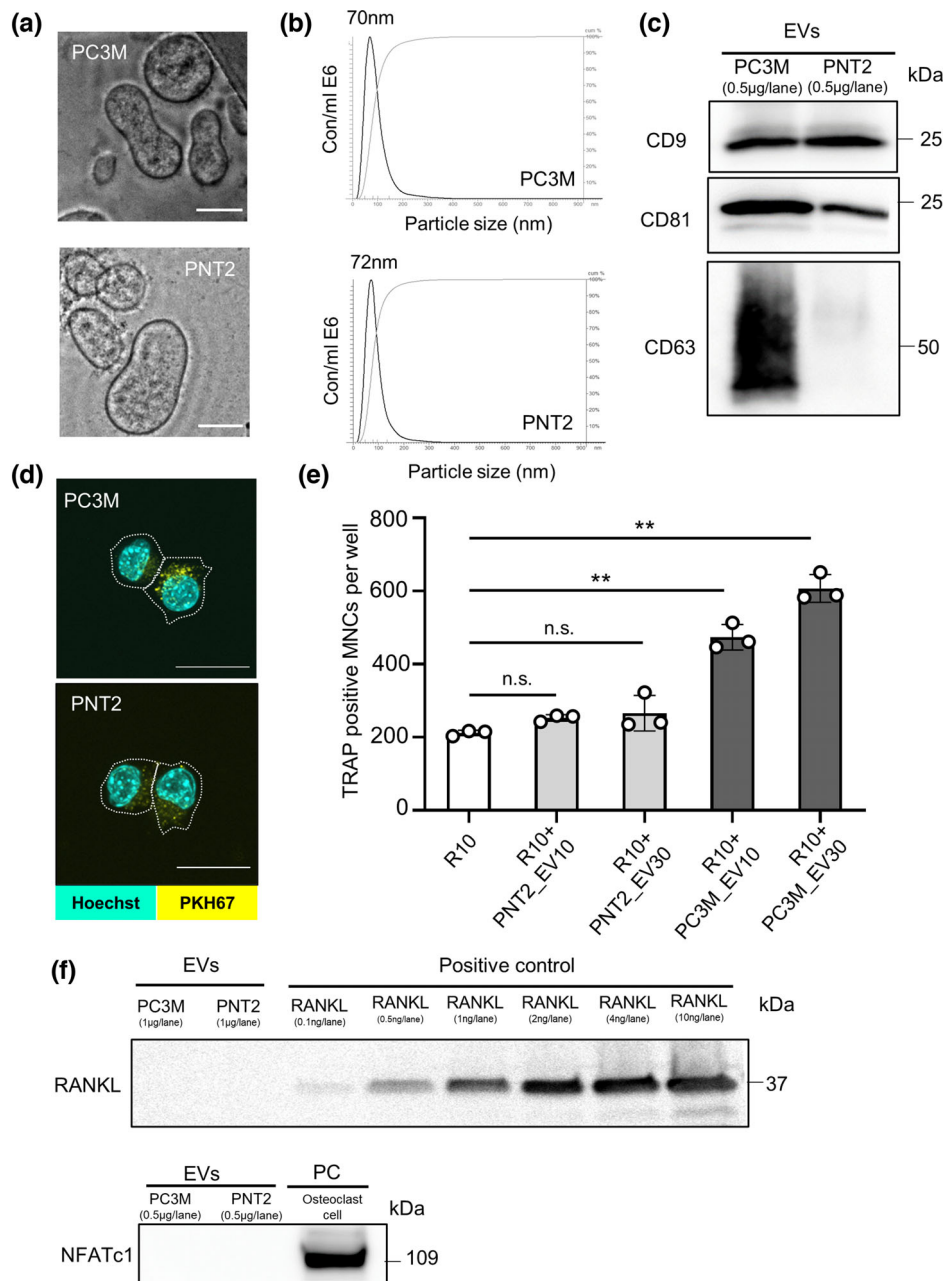


FIGURE 3 Prostate cancer-derived EVs specifically promote osteoclastogenesis. (a) Representative images of EVs isolated from PC3M and PNT2 cells and observed under transmission electron microscopy. Scale bar, 100 nm. (b) The particle size distributions and concentrations of EVs from PC3M and PNT2 cells were measured using a NanoSight nanoparticle tracking system. (c) EVs from PC3M and PNT2 cells were analysed by immunoblotting using anti-CD9, anti-CD63, and anti-CD81 antibodies. (d) Representative confocal microscopy images. EVs derived from PC3M and PNT2 cells were labelled with PKH67 and added to osteoclast precursors in the presence of RANKL (10 ng/mL). White dots indicate cell morphologies. Scale bars, 25 μ m. (e) Analysis of the effect of EVs derived from PC3M and PNT2 cells on osteoclast precursors (RAW264.7 cells). EVs were added to RAW264.7 cells, and osteoclast differentiation was evaluated by tartrate-resistant acid phosphatase (TRAP) staining after 96 h. The number of TRAP-positive multinucleated cells containing more than 3 nuclei (MNCs) was counted. (f) EVs from PC3M and PNT2 cells were analysed by immunoblotting using anti-RANKL and anti-NFATc1 antibodies. As positive controls, recombinant RANKL and cell lysates from osteoclast cells that were differentiated from RAW264.7 cells were used. R10 represents 10 ng/mL RANKL, EV10 represents 10 μ g/mL EVs and EV30 represents 30 μ g/mL EVs. Error bars represent s.d. of triplicate experiments, with significant differences determined by Dunnett's test (** $p < 0.01$)

RANKL. By immunoblotting, we verified that CDCP1 expression in PC3M-derived EVs was higher than that in PNT2-derived EVs (Figure 4f).

As CDCP1 is a transmembrane protein (Harrington et al., 2016), the endogenous localization and expression level of CDCP1 on or in EVs were evaluated, as shown in Figure 4g. The immunoelectron microscopy images illustrated the localization of CDCP1 on the surface of PC3M- and PNT2-derived EVs. Although many dots were observed on PC3M-derived EVs, only one dot was

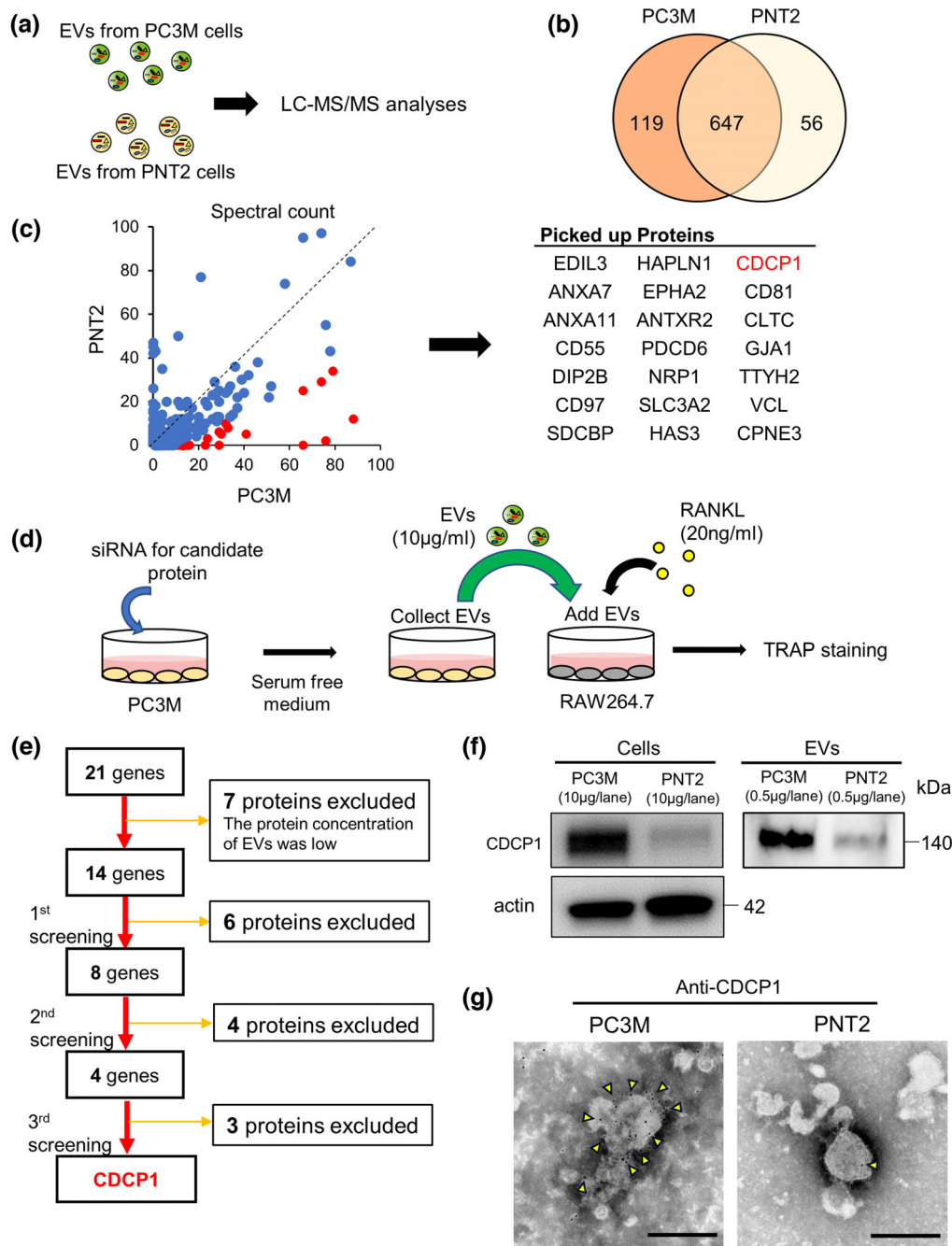


FIGURE 4 Screening of molecules expressed on EVs that promote osteoclastogenesis. (a) Schematic representation of the proteome analysis of PC3M- and PNT2-derived EVs. (b) Venn diagram of the number of detected proteins in PC3M- and PNT2-derived EVs. (c) Analysis of LC-MS/MS data by spectral count in PC3M- and PNT2-derived EVs. Twenty-one proteins that were significantly enriched in PC3M-derived EVs were selected as candidate proteins to promote osteoclast differentiation (Fisher's exact test; $p < 0.003$). (d) Schematic protocol for small-scale screening using the siRNA SMART pool in PC3M cells to detect candidate proteins that promote osteoclast differentiation. (e) Flow diagram of proteins used for selecting the candidate protein CDCP1. (f) EVs from PC3M and PNT2 cells were analysed by immunoblotting using an anti-human CDCP1 antibody. Proteins from whole cell lysates or EVs were separated on SDS-PAGE gels, followed by immunoblotting. A 10 µg cell lysate sample was used for the detection of CDCP1 and actin. A 0.5 µg EV protein sample was used for the detection of CDCP1. (g) Immunoelectron microscopy images of PC3M EVs and PNT2 EVs labelled with anti-CDCP1 antibody. The black dots emphasized by yellow arrows indicate the presence of CDCP1. Scale bar, 200 nm.

observed on PNT2-derived EVs (Figure 4g). The reduction in CDCP1 expression in EVs after transfection with CDCP1 siRNA was also confirmed (Figure S4b). CDCP1 siRNA had no effect on total CD9 or CD63 expression in EVs derived from PC3M cells (Figure S4b). These results suggest that CDCP1 located on EVs (CDCP1 on EVs) is a specific molecule that promotes mature osteoclast formation in the presence of RANKL.

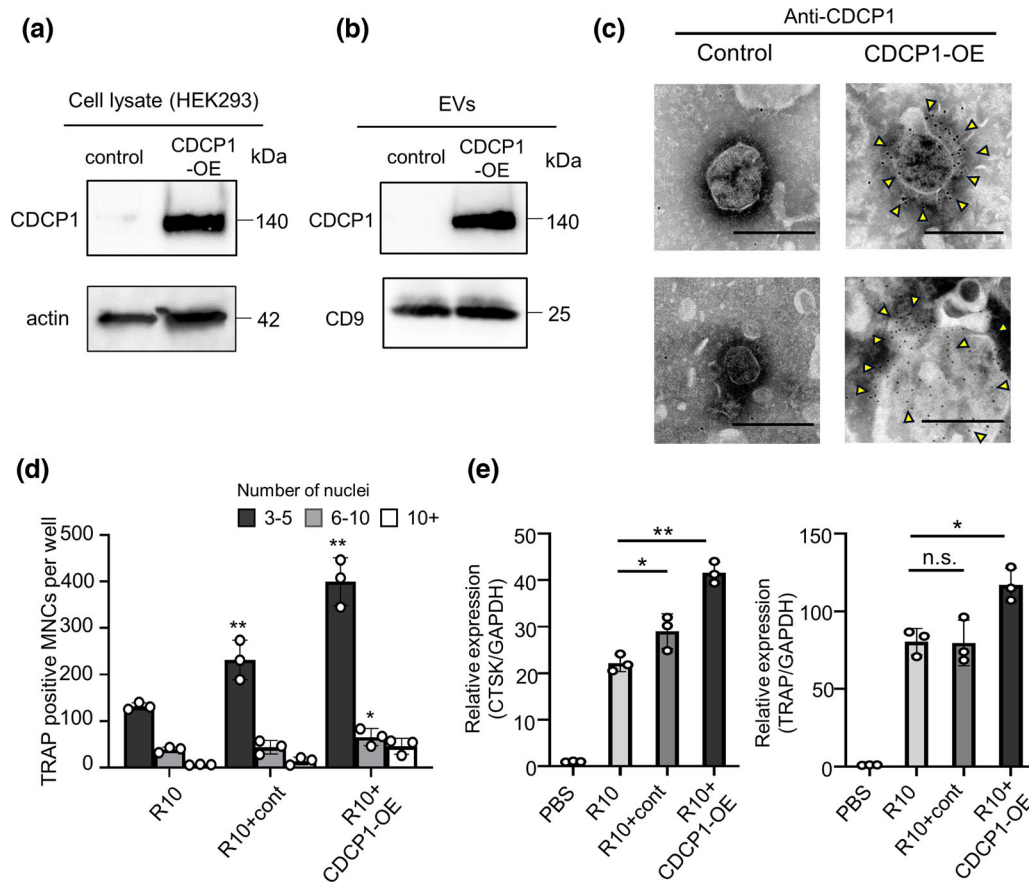


FIGURE 5 CDCP1 located on EVs is a key molecule for osteoclastogenesis. (a) Cell lysates from HEK293 cells overexpressing CDCP1 or the control were analysed by immunoblotting using anti-CDCP1 and anti-actin antibodies. Actin was used as the loading control. (b) EVs from HEK293 cells overexpressing CDCP1 or the control were analysed by immunoblotting using anti-CDCP1 and anti-CD9 antibodies. CD9 was used as the loading control. (c) Immunoelectron microscopy images of HEK293 cell-derived EVs labelled with anti-CDCP1 antibody. The black dots emphasized by yellow arrows indicate the presence of CDCP1. Scale bar, 200 nm. (d) Osteoclast precursor cells were cultured with EVs derived from HEK293 control cells (control) or CDCP1-overexpressing HEK293 (CDCP1-OE)-derived EVs (30 $\mu\text{g}/\text{mL}$) in the presence of RANKL (10 ng/mL). At the end of Day 4, osteoclast precursor-induced cells were fixed and stained for TRAP, and the number of TRAP-positive multinucleated cells containing more than 3 nuclei (MNCs) was counted. (e) Quantitative PCR analysis was performed for markers of osteoclast differentiation, including TRAP and CTSK. Error bars represent s.d. of triplicate experiments. ** indicates a significant difference from the RANKL-stimulated group (R10) as determined by Dunnett's test ($*p < 0.05$, $**p < 0.01$). R10 represents 10 ng/mL RANKL.

3.5 | CDCP1 on EVs is a key molecule that promotes osteoclastogenesis

To confirm the role of CDCP1 on EVs, we examined the biological effects of CDCP1-overexpressing EVs on osteoclastogenesis. To further test whether CDCP1 promotes osteoclastogenesis, we stably overexpressed CDCP1 in HEK293 cells with low basal levels of CDCP1 (Figure 5a). CDCP1 was detected in EVs isolated from the culture medium of CDCP1-overexpressing HEK293 cells by immunoblotting (Figure 5b). We also confirmed that CDCP1 was located on the surface of EVs by immunoelectron microscopy (Figure 5c). In addition, CDCP1-overexpressing HEK293-derived EVs accelerated mature osteoclast formation compared with control EVs in the presence of RANKL (Figure 5d). To confirm the effect of EVs derived from CDCP1-overexpressing HEK293 cells on osteoclastogenesis, possible transcriptional regulation induced by EVs was analysed by qRT-PCR. When osteoclast precursor (RAW264.7) cells were incubated for 96 h with the combination of RANKL and CDCP1-overexpressing HEK293-derived EVs, increased mRNA levels of several markers of osteoclast formation and activity were observed, including TRAP and CTSK (Figure 5e).

The effects of CDCP1 on EVs on mature osteoclast formation were also confirmed in primary osteoclast precursor cells. We prepared osteoclast precursors as shown above and found that CDCP1-overexpressing HEK293-derived EVs significantly promoted mature osteoclast formation in the presence of RANKL (Figure S5a), and this phenotype was confirmed by qRT-PCR (Figure S5b).

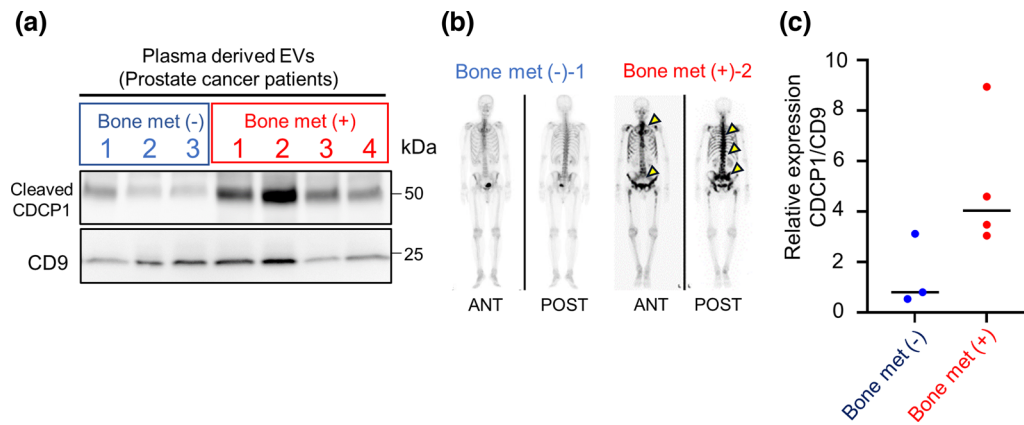


FIGURE 6 The CDCPI protein is detected in EVs derived from metastatic prostate cancer patients. (a) Immunoblotting for CDCPI protein expression levels in EVs derived from nonmetastatic and bone metastatic prostate cancer patients. Each lane was loaded with EVs from 100 μ L plasma. (b) The results of bone scintigraphy of representative cases. (c) Quantification of the relative expression levels of CDCPI protein normalized to CD9 in EVs.

3.6 | CDCPI is present in the plasma-derived EVs of metastatic prostate cancer patients

Finally, to determine whether CDCPI could be detected in metastatic PCa patients, we used ultracentrifugation to isolate EVs from three human plasma samples derived from nonmetastatic PCa patients and four from bone metastatic PCa patients. Immunoblotting was performed to examine the expression level of CDCPI protein in these samples. Each lane was loaded with EVs from 100 μ L plasma. The results showed that EVs derived from bone metastatic PCa patients had significantly higher expression of CDCPI than those derived from nonmetastatic PCa patients (Figures 6a and S6a). The results of bone scintigraphy in representative cases are shown in Figure 6b. In addition, the relative expression level of CDCPI normalized by CD9 tended to be higher in bone metastatic PCa patients (Figure 6c). These data suggested that EV-associated CDCPI has the potential to predict bone metastases in PCa patients. In addition, the overall survival of PCa patients is usually longer (Hamdy et al., 2016), so it was difficult to predict their prognosis using the expression of CDCPI. However, in other cancers that frequently metastasize to bone, such as renal clear cell carcinoma (Grünwald et al., 2018), lung adenocarcinoma (Kuchuk et al., 2015) and head-neck squamous cell carcinoma (Sakisuka et al., 2021), CDCPI was a significant prognostic factor (Figure S7).

4 | DISCUSSION

The frequent occurrence of bone metastases in PCa patients is the leading cause of mortality as well as loss in quality of life. However, the molecular mechanisms that mediate the process of bone metastasis remain poorly defined. An ever-increasing number of studies have demonstrated that EVs modulate cancer progression (Wortzel et al., 2019). Indeed, previous reports have shown that EVs from PCa cells promote proliferation (Hosseini-Beheshti et al., 2016), modulate the immune system (Lundholm et al., 2014) and confer drug resistance (Corcoran et al., 2012). Although PCa frequently presents with osteoblastic bone, previous reports have shown the importance of osteoclasts in PCa bone metastasis (Yonou et al., 2004; Zhang et al., 2001). In addition, Shimazaki et al. (1992) reported that the osteolytic bone metastasis population of PCa had a worse prognosis than the osteoblastic phenotype. Thus, the role of osteoclasts in PCa bone metastasis is worth investigating. In this study, we investigated the role of EVs secreted by bone metastatic PCa cells and first found that EVs from PCa promote mature osteoclast formation in the presence of RANKL. In contrast, the addition of EVs from PCa alone did not result in mature osteoclast formation. As shown in Figure S3a, RANKL has a robust effect on osteoclast differentiation and is the essential cue for osteoclast differentiation. However, after the addition of EVs from PCa, single nucleus TRAP positive cells were observed. This suggests that EVs from PCa alone do not have sufficient power to lead to mature osteoclast formation but rather provide a supportive effect.

Using functional siRNA screening, we determined that CDCPI on EVs is responsible for the mature osteoclast formation. CDCPI is a transmembrane cellular receptor that is reported to have a role in regulating tumour progression to metastasis. Indeed, in PCa, several studies reported the role of CDCPI in tumour progression. Functional blocking antibodies inhibited CDCPI-triggered survival of PCa and decreased metastatic colonization in the lung (Deryugina et al., 2009; Fukuchi et al., 2010; Siva et al., 2008). In addition to PCa cell-associated CDCPI, CDCPI is also reported to be released from PC3 cells via EVs (Sandvig & Llorente, 2012). However, the localization and functional roles of CDCPI on EVs have not been reported. In this study, we identified that CDCPI is secreted via EVs and revealed the novel role of CDCPI on EVs. We revealed that overexpression of

CDCP1 on EVs derived from HEK293 cells, which have low basal levels of CDCP1, promoted mature osteoclast formation in the presence of RANKL.

Recent studies have also emphasized the importance of the microenvironment in cancer therapy. For instance, as demonstrated in clinical trials, several drugs, such as denosumab (Coleman et al., 2012) and odanacatib (Clézardin, 2011), target microenvironment cytokines to inhibit the progression of bone metastasis. However, these therapies do not completely inhibit the progression of bone metastasis. Previous reports have shown that miRNA or mRNA contained in EVs affect the tumour microenvironment and contribute to tumour progression (Tominaga et al., 2015; Yokoi et al., 2017). However, it is difficult to directly target these molecules in the circulation because they are packaged in EVs. On the contrary, we previously reported that administration of human-specific antibodies against CD9 or CD63, which are enriched on the surface of EVs, decreased metastasis of breast cancer in vivo (Nishida-Aoki et al., 2017). In this study, we elucidated the intercellular communication between PCa cells and osteoclasts through transfer of CDCP1 localized on EVs. Therefore, while further investigation would be required, this communication could be a direct therapeutic target in future PCa management.

Current diagnostics of bone metastatic disease in PCa are not sufficient to provide early detection or regular monitoring for the improvement of treatment management. In addition, novel diagnostic methods are needed because current diagnostics, based on imaging procedures, are costly and could cause patient harm as a result of radiation exposure. The present study found higher CDCP1 expression in plasma EVs derived from PCa patients with bone metastasis compared with localized tumours. Our data suggest that CDCP1 on EVs may be a useful marker for predicting the likelihood of metastases to bone in PCa patients. Indeed, CDCP1 is reported to be highly expressed in CRPC (Zhao et al., 2022), and CDCP1 is known to contribute to metastasis in PTEN-deficient PCa (Alajati et al., 2020). The expression level of CD9, a common EV marker, in EVs was not significantly different between bone metastatic and nonmetastatic PCa patients (Figure S6b); therefore, we normalized the expression level of CDCP1 to CD9 and found that the relative expression of CDCP1 tended to be higher in bone metastatic PCa patients (Figure 6c). These results indicate that CDCP1 on EVs might be useful to detect bone metastasis in PCa. Furthermore, interestingly, the expression of CDCP1 was a significant factor in other cancers that frequently show osteolytic bone metastasis; thus, our findings might be applicable to not only PCa but also other kinds of cancers.

In summary, this is the first experimental record reporting a role of CDCP1 located on EVs in osteoclastogenesis. Currently, EV research is progressing to include studies on clinical applications for diagnosis or therapeutics. Our insights into the mechanisms of osteoclastogenesis may provide future opportunities for therapeutic intervention and the detection of bone metastasis. We hope that these findings can lead to an improvement in clinical outcomes for advanced PCa patients.

AUTHOR CONTRIBUTIONS

Fumihiko Urabe: Conceptualization; Data curation; Formal analysis; Investigation; Methodology; Visualization; Writing-original draft. **Nobuyoshi Kosaka:** Conceptualization; Methodology; Validation; Writing-original draft. **Yusuke Yamamoto:** Supervision; Visualization; Writing-review & editing. **Kagenori Ito:** Data curation; Investigation; Validation; Writing-original draft. **Kurataka Otsuka:** Supervision; Writing-original draft; Supporting. **Carolina Soekmadji:** Supervision; Supporting, Writing-original draft. **Shin Egawa:** Writing-original draft. **Takahiro Kimura:** Supervision; Visualization; Writing-original draft. **Takahiro Ochiya:** Conceptualization; Funding acquisition; Investigation; Methodology; Supervision; Writing-original draft.

ACKNOWLEDGEMENTS

We thank Yurika Sawa (Tokyo Medical University) and Ari Miura (Boston University) for technical support for this work. We also thank Shunsuke Tsuzuki, Kazuhiro Maeda, Mitsuru Saito, Koji Asano (The Jikei University), Tomofumi Yamamoto, Fumitaka Takeshita (National Cancer Center) and members of the Department of Molecular and Cellular Medicine (Tokyo Medical University) for critical discussion regarding this manuscript. This work was supported by Japan Agency for Medical Research and Development, AMED (JP21cm0106402), Researcher Promotion Grant from the Japanese Foundation for Prostate Research, Young Researcher Promotion Grant from Japanese Urological Association, Grant-in-Aid for Young Scientists from the Japan Society for the Promotion of Science, JSPS (21K16758), and the Office of the Assistant Secretary of Defence for Health Affairs through the US Department of Defence Congressionally Directed Medical Research Program Prostate Cancer Research Program Idea Development Award (W81XWH-16-1-0736).

CONFLICT OF INTEREST STATEMENT

The authors have declared that no conflict of interest exists.

ORCID

Fumihiko Urabe  <https://orcid.org/0000-0002-2599-8183>

Carolina Soekmadji  <https://orcid.org/0000-0002-6920-6627>

Takahiro Ochiya  <https://orcid.org/0000-0002-0776-9918>

REFERENCES

- Alajati, A., D'ambrosio, M., Troiani, M., Mosole, S., Pellegrini, L., Chen, J., Revandkar, A., Bolis, M., Theurillat, J.-P., Guccini, I., Losa, M., Calcinotto, A., De Bernardis, G., Pasquini, E., D'antuono, R., Sharp, A., Figueiredo, I., Nava Rodrigues, D., Welti, J., ... Alimonti, A. (2020). CDCP1 overexpression drives prostate cancer progression and can be targeted in vivo. *Journal of Clinical Investigation*, *130*(5), 2435–2450.
- Boyle, W. J., Simonet, W. S., & Lacey, D. L. (2003). Osteoclast differentiation and activation. *Nature*, *423*(6937), 337–342.
- Clézardin, P. (2011). Therapeutic targets for bone metastases in breast cancer. *Breast Cancer Research*, *13*(2), 207.
- Coleman, R., Gnant, M., Morgan, G., & Clezardin, P. (2012). Effects of bone-targeted agents on cancer progression and mortality. *JNCI: Journal of the National Cancer Institute*, *104*(14), 1059–1067.
- Corcoran, C., Rani, S., O'Brien, K., O'Neill, A., Prencipe, M., Sheikh, R., Webb, G., Mcdermott, R., Watson, W., Crown, J., & O'driscoll, L. (2012). Docetaxel-resistance in prostate cancer: Evaluating associated phenotypic changes and potential for resistance transfer via exosomes. *PLoS ONE*, *7*(12), e50999.
- Deryugina, E. I., Conn, E. M., Wortmann, A., Partridge, J. J., Kupriyanova, T. A., Ardi, V. C., Hooper, J. D., & Quigley, J. P. (2009). Functional role of cell surface CUB domain-containing protein 1 in tumor cell dissemination. *Molecular Cancer Research*, *7*(8), 1197–1211.
- Fukuchi, K., Steiniger, S. C. J., Deryugina, E., Liu, Y., Lowery, C. A., Gloeckner, C., Zhou, B., Kaufmann, G. F., Quigley, J. P., & Janda, K. D. (2010). Inhibition of tumor metastasis: functional immune modulation of the CUB domain containing protein 1. *Molecular Pharmaceutics*, *7*(1), 245–253.
- Grünwald, V., Eberhardt, B., Bex, A., Flörcken, A., Gauler, T., Derlin, T., Panzica, M., Dürr, H. R., Grötz, K. A., Giles, R. H., Von Falck, C., Graser, A., Muacevic, A., & Staehler, M. (2018). An interdisciplinary consensus on the management of bone metastases from renal cell carcinoma. *Nature Reviews Urology*, *15*(8), 511–521.
- Guise, T. A., Mohammad, K. S., Clines, G., Stebbins, E. G., Wong, D. H., Higgins, L. S., Vessella, R., Corey, E., Padalecki, S., Suva, L., & Chirgwin, J. M. (2006). Basic mechanisms responsible for osteolytic and osteoblastic bone metastases. *Clinical Cancer Research*, *12*(20 Pt 2), 6213s–6216s.
- Hamdy, F. C., Donovan, J. L., Lane, J. A., Mason, M., Metcalfe, C., Holding, P., Davis, M., Peters, T. J., Turner, E. L., Martin, R. M., Oxley, J., Robinson, M., Staffurth, J., Walsh, E., Bollina, P., Catto, J., Doble, A., Doherty, A., Gillatt, D., ... Neal, D. E. (2016). 10-Year Outcomes after Monitoring, Surgery, or Radiotherapy for Localized Prostate Cancer. *New England Journal of Medicine*, *375*(15), 1415–1424.
- Harrington, B. S., He, Y., Davies, C. M., Wallace, S. J., Adams, M. N., Beaven, E. A., Roche, D. K., Kennedy, C., Chetty, N. P., Crandon, A. J., Flatley, C., Oliveira, N. B., Shannon, C. M., Defazio, A., Tinker, A. V., Gilks, C. B., Gabrielli, B., Brennan, D. J., Coward, J. I., ... Hooper, J. D. (2016). Cell line and patient-derived xenograft models reveal elevated CDCP1 as a target in high-grade serous ovarian cancer. *British Journal of Cancer*, *114*(4), 417–426.
- Hosseini-Beheshti, E., Choi, W., Weiswald, L.-B., Kharmate, G., Ghaffari, M., Roshan-Moniri, M., Hassona, M. D., Chan, L., Chin, M. Y., Tai, I. T., Rennie, P. S., Fazli, L., & Guns, E. S. T. (2016). Exosomes confer pro-survival signals to alter the phenotype of prostate cells in their surrounding environment. *Oncotarget*, *7*(12), 14639–14658.
- Irie, A., Yamamoto, K., Miki, Y., & Murakami, M. (2017). Phosphatidylethanolamine dynamics are required for osteoclast fusion. *Scientific Reports*, *7*, 46715.
- Kingsley, L. A., Fournier, P. G. J., Chirgwin, J. M., & Guise, T. A. (2007). Molecular biology of bone metastasis. *Molecular Cancer Therapeutics*, *6*(10), 2609–2617.
- Kosaka, N., Iguchi, H., Hagiwara, K., Yoshioka, Y., Takeshita, F., & Ochiya, T. (2013). Neutral sphingomyelinase 2 (nSMase2)-dependent exosomal transfer of angiogenic microRNAs regulate cancer cell metastasis. *Journal of Biological Chemistry*, *288*(15), 10849–10859.
- Kuchuk, M., Kuchuk, I., Sabri, E., Hutton, B., Clemons, M., & Wheatley-Price, P. (2015). The incidence and clinical impact of bone metastases in non-small cell lung cancer. *Lung Cancer*, *89*(2), 197–202.
- Lundholm, M., Schröder, M., Nagaeva, O., Baranov, V., Widmark, A., Mincheva-Nilsson, L., & Wikström, P. (2014). Prostate tumor-derived exosomes down-regulate NKG2D expression on natural killer cells and CD8+ T cells: Mechanism of immune evasion. *PLoS ONE*, *9*(9), e108925.
- Matsumoto, M., Kogawa, M., Wada, S., Takayanagi, H., Tsujimoto, M., Katayama, S., Hisatake, K., & Nogi, Y. (2004). Essential role of p38 mitogen-activated protein kinase in cathepsin K gene expression during osteoclastogenesis through association of NFATc1 and PU.1. *Journal of Biological Chemistry*, *279*(44), 45969–45979.
- Matsuo, K., & Irie, N. (2008). Osteoclast-osteoblast communication. *Archives of Biochemistry and Biophysics*, *473*(2), 201–209.
- Nishida-Aoki, N., Tominaga, N., Takeshita, F., Sonoda, H., Yoshioka, Y., & Ochiya, T. (2017). Disruption of Circulating Extracellular Vesicles as a Novel Therapeutic Strategy against Cancer Metastasis. *Molecular Therapy*, *25*(1), 181–191.
- Peng, L., Kapp, E. A., Mclauchlan, D., & Jordan, T. W. (2011). Characterization of the Asia Oceania Human Proteome Organisation Membrane Proteomics Initiative Standard using SDS-PAGE shotgun proteomics. *Proteomics*, *11*(22), 4376–4384.
- Sakisuka, T., Kashiwagi, N., Doi, H., Takahashi, H., Arisawa, A., Matsuo, C., Masuda, Yu., Inohara, H., Sato, K., Outani, H., Ishii, K., & Tomiyama, N. (2021). Prognostic factors for bone metastases from head and neck squamous cell carcinoma: A case series of 97 patients. *Molecular and Clinical Oncology*, *15*(5), 246.
- Sandvig, K., & Llorente, A. (2012). Proteomic analysis of microvesicles released by the human prostate cancer cell line PC-3. *Molecular & Cellular Proteomics*, *11*(7), M111.012914–1–M111.012914–11.
- Shimazaki, J., Higa, T., Akimoto, S., Masai, M., & Isaka, S. (1992). Clinical course of bone metastasis from prostatic cancer following endocrine therapy: Examination with bone x-ray. *Advances in Experimental Medicine and Biology*, *324*, 269–275.
- Siegel, R. L., Miller, K. D., Fuchs, H. E., & Jemal, A. (2021). Cancer Statistics, 2021. *CA: A Cancer Journal for Clinicians*, *71*(1), 7–33.
- Siva, A. C., Wild, M. A., Kirkland, R. E., Nolan, M. J., Lin, B., Maruyama, T., Yantiri-Wernimont, F., Frederickson, S., Bowdish, K. S., & Xin, H. (2008). Targeting CUB domain-containing protein 1 with a monoclonal antibody inhibits metastasis in a prostate cancer model. *Cancer Research*, *68*(10), 3759–3766.
- Smith, M. R., Saad, F., Coleman, R., Shore, N., Fizazi, K., Tombal, B., Miller, K., Sieber, P., Karsh, L., Damião, R., Tammela, T. L., Egerdie, B., Van Poppel, H., Chin, J., Morote, J., Gómez-Veiga, F., Borkowski, T., Ye, Z., Kupic, A., ... Goessl, C. (2012). Denosumab and bone-metastasis-free survival in men with castration-resistant prostate cancer: Results of a phase 3, randomised, placebo-controlled trial. *Lancet*, *379*(9810), 39–46.
- Song, R. L., Liu, X. Z., Zhu, J. Q., Zhang, J. M., Gao, Q., Zhao, H. Y., Sheng, A. Z., Yuan, Y., Gu, J. H., Zou, H., Wang, Q. C., & Liu, Z. P. (2014). New roles of filopodia and podosomes in the differentiation and fusion process of osteoclasts. *Genetics and Molecular Research [Electronic Resource]*, *13*(3), 4776–4787.
- Sturge, J., Caley, M. P., & Waxman, J. (2011). Bone metastasis in prostate cancer: Emerging therapeutic strategies. *Nature reviews Clinical oncology*, *8*(6), 357–368.
- Teitelbaum, S. L., & Ross, F. P. (2003). Genetic regulation of osteoclast development and function. *Nature Reviews Genetics*, *4*(8), 638–649.
- Tominaga, N., Kosaka, N., Ono, M., Katsuda, T., Yoshioka, Y., Tamura, K., Lötvall, J., Nakagama, H., & Ochiya, T. (2015). Brain metastatic cancer cells release microRNA-181c-containing extracellular vesicles capable of destructing blood-brain barrier. *Nature Communications*, *6*, 6716.
- Urabe, F., Patil, K., Ramm, G. A., Ochiya, T., & Soekmadji, C. (2021). Extracellular vesicles in the development of organ-specific metastasis. *Journal of Extracellular Vesicles*, *10*(9), e12125.
- Valadi, H., Ekström, K., Bossios, A., Sjöstrand, M., Lee, J. J., & Lötvall, J. O. (2007). Exosome-mediated transfer of mRNAs and microRNAs is a novel mechanism of genetic exchange between cells. *Nature Cell Biology*, *9*(6), 654–659.
- Wortzel, I., Dror, S., Kenific, C. M., & Lyden, D. (2019). Exosome-Mediated Metastasis: Communication from a Distance. *Developmental Cell*, *49*(3), 347–360.

- Yagi, M., Miyamoto, T., Toyama, Y., & Suda, T. (2006). Role of DC-STAMP in cellular fusion of osteoclasts and macrophage giant cells. *Journal of Bone and Mineral Metabolism*, 24(5), 355–358.
- Yamanaka, H., Takeyoshi, M., Minobe, Y., Yakabe, Y., Takatsuki, M., & Sato, H. (2007). Comprehensive identification of cytochrome p450 isoforms from solubility-based fractionated rat liver microsomes. *Drug Metabolism Letters*, 1(4), 281–286.
- Yokoi, A., Yoshioka, Y., Yamamoto, Y., Ishikawa, M., Ikeda, S.-I., Kato, T., Kiyono, T., Takeshita, F., Kajiyama, H., Kikkawa, F., & Ochiya, T. (2017). Malignant extracellular vesicles carrying MMP1 mRNA facilitate peritoneal dissemination in ovarian cancer. *Nature Communications*, 8, 14470.
- Yonou, H., Ochiai, A., Goya, M., Kanomata, N., Hokama, S., Morozumi, M., Sugaya, K., Hatano, T., & Ogawa, Y. (2004). Intraosseous growth of human prostate cancer in implanted adult human bone: Relationship of prostate cancer cells to osteoclasts in osteoblastic metastatic lesions. *Prostate*, 58(4), 406–413.
- Yoshioka, Y., Konishi, Y., Kosaka, N., Katsuda, T., Kato, T., & Ochiya, T. (2013). Comparative marker analysis of extracellular vesicles in different human cancer types. *Journal of Extracellular Vesicles*, 2, 20424.
- Yuen, H.-F., Chiu, Y.-T., Chan, K.-K., Chan, Y.-P., Chua, C.-W., McCrudden, C. M., Tang, K.-H., El-Tanani, M., Wong, Y.-C., Wang, X., & Chan, K.-W. (2010). Prostate cancer cells modulate osteoblast mineralisation and osteoclast differentiation through Id-1. *British Journal of Cancer*, 102(2), 332–341.
- Zhang, J., Dai, J., Qi, Y., Lin, D.-L., Smith, P., Strayhorn, C., Mizokami, A., Fu, Z., Westman, J., & Keller, E. T. (2001). Osteoprotegerin inhibits prostate cancer-induced osteoclastogenesis and prevents prostate tumor growth in the bone. *Journal of Clinical Investigation*, 107(10), 1235–1244.
- Zhao, N., Chopra, S., Trepka, K., Wang, Y.-H., Sakhamuri, S., Hooshdaran, N., Kim, H., Zhou, J., Lim, S. A., Leung, K. K., Egusa, E. A., Zhu, J., Zhang, Li., Foye, A., Sriram, R., Chan, E., Seo, Y., Feng, F. Y., Small, E. J., ... Evans, M. J. (2022). CUB Domain-Containing Protein 1 (CDCP1) Is a Target for Radioligand Therapy in Castration-Resistant Prostate Cancer, including PSMA Null Disease. *Clinical Cancer Research*, 28(14), 3066–3075.

SUPPORTING INFORMATION

Additional supporting information can be found online in the Supporting Information section at the end of this article.

How to cite this article: Urabe, F., Kosaka, N., Yamamoto, Y., Ito, K., Otsuka, K., Soekmadji, C., Egawa, S., Kimura, T., & Ochiya, T. (2023). Metastatic prostate cancer-derived extracellular vesicles facilitate osteoclastogenesis by transferring the CDCP1 protein. *Journal of Extracellular Vesicles*, 12, e12312. <https://doi.org/10.1002/jev2.12312>